Examen 2020-2021
Cours de Micro-nano-biotechnologie – Vincent MANSARD

L'examen portera sur l'article ci joint et comportera des questions sur le cours (à l'exception du cours de Mercredi 25 octobre) :

Rapid Diagnostic for Point-of-Care Malaria Screening
Samantha E. McBirney, Dongyu Chen, Alexis Scholtz, Hossein Ameri and Andrea M. Armani
DOI: 10.1021/acssensors.8b00269 ACS Sens. 2018, 3, 1264−1270

Prenez soin de bien lire l'article, de bien comprendre les termes clefs et bien comprendre l'analyse des résultats. L'article fait plusieurs fois référence au « Suplementary Information (SI) ». C'est un PDF accessible en ligne donnant des informations moins importantes. La lecture des SI n'est pas attendue. Vous pouvez y jeter un œil si vous avez le sentiments que cela vous aide à la compréhension de l'article.

Documents autorisés :
article (6 pages qui peuvent annotées) + 1 page de notes personnelles

La capacité à fournir des réponses simples, claires et bien écrites est une compétence importante. L'évaluation en tiendra fortement compte. Les étudiants peu à l'aise en français pourront répondre en anglais. Cependant le mélange des deux langues ne sera pas accepté.

ACS SENSORS

Letter

Cite This: ACS Sens. 2018, 3, 1264−1270

pubs.acs.org/acssensors

Rapid Diagnostic for Point-of-Care Malaria Screening

Samantha E. McBirney,[†] Dongyu Chen,[‡] Alexis Scholtz,[§] Hossein Ameri,[∥] and Andrea M. Armani*[,⊥]

[†]Department of Biomedical Engineering, [‡]Ming Hsieh Department of Electrical Engineering-Electrophysics, and [⊥]Mork Family Department of Chemical Engineering and Materials Science, University of Southern California, Los Angeles, California 90089, United States

[§]Department of Biomedical Engineering, Johns Hopkins University, Baltimore, Maryland 21218, United States

[∥]USC Roski Eye Institute, Department of Ophthalmology, Keck School of Medicine of the University of Southern California, Los Angeles, California 90033, United States

Supporting Information

ABSTRACT: Despite significant success in therapeutic development, malaria remains a widespread and deadly infectious disease in the developing world. Given the nearly 100% efficacy of current malaria therapeutics, the primary barrier to eradication is lack of early diagnosis of the infected population. However, there are multiple strains of malaria. Although significant efforts and resources have been invested in developing antibody-based diagnostic methods for *Plasmodium falciparum*, a rapid and easy to use screening method capable of detecting all malaria strains has not been realized. Yet, until the entire malaria-infected population receives treatment, the disease will continue to impact society. Here, we report the development of a portable, magneto-optic technology for early stage malaria diagnosis based on the detection of the malaria pigment, hemozoin. Using β-hematin, a hemozoin mimic, we demonstrate detection limits of <0.0081 μg/mL in 500 μL of whole rabbit blood with no additional reagents required. This level corresponds to <26 parasites/μL, a full order of magnitude below clinical relevance and comparable to or less than existing technologies.

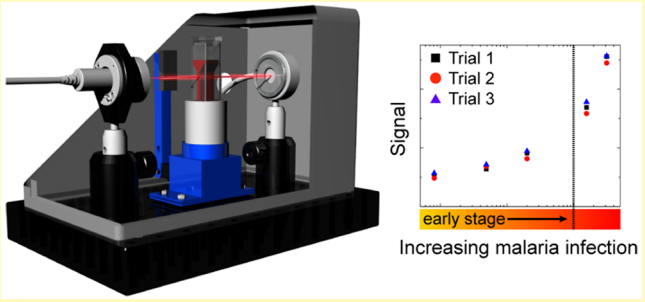

KEYWORDS: *malaria, hemozoin, biosensors, portable diagnostics, label-free detection*

Malaria remains a major global health problem. It is the leading cause of morbidity and mortality. However, although malaria is found in nearly every country, the burden of the disease rests primarily in the developing world. Nearly half of the world's population currently lives in malaria-endemic regions.[1] Each year, more than 200 million people are infected, and more than 500,000 individuals die from malaria and its complications.[2−7] Seventy percent of deaths occur in children aged under 5 years.[7] These rates are particularly frustrating given the efficacy of current therapeutics. Specifically, if an infected person is identified early, treatment is nearly 100% effective when properly prescribed and administered.[8−11] Therefore, to eradicate malaria, it is necessary to identify and treat the infected population.

The two most commonly used methods are optical microscopy and antibody-based diagnostic tests. Light microscopy of blood smears has been the gold standard for malaria diagnosis for over a century.[8,9,12,13] Among methods currently used, it is the most reliable at identifying infections from all malaria parasites. However, it is low-throughput and is both labor-intensive and expensive as it requires the use of high-powered microscopes.[1,14,15] Additionally, the reliability of the method is strongly dependent on the technician's training and experience, with accuracy varying by several orders of magnitude. This level of user bias in a diagnostic is clearly an issue and motivated the development of the rapid diagnostic test (RDT). Since the initial demonstration, species-specific RDTs have been designed based on the different proteins and biomarkers. For example, RDTs detecting the presence of histidine-rich protein 2 (HRP-2) (specific to *Plasmodium falciparum*), *Plasmodium* lactate dehydrogenase (specific to *P. vivax*, *P. malariae*, and *P. ovale*) and/or aldolase (a panmalarial antigen found in all *Plasmodium* species)[16−21] have been demonstrated. However, like any antigen-based diagnostic, reliability is governed by stability of the reagent(s), which, in a low-resource environment, is a fundamental concern.[22] In addition, the accuracy of these antibodies in malaria detection has recently been called into question.[23] Therefore, developing a screen for malaria that is independent of user bias is clearly of great societal interest and need.

At the heart of any diagnostic test is an indicator of the disease. Initially called the malaria pigment,[24] hemozoin is a magnetic nanoparticle byproduct of the parasite.[25−30] Because it is specific to malaria, it is an ideal biomarker. Notably, unlike

Received: March 31, 2018
Accepted: May 18, 2018
Published: May 21, 2018

DOI: 10.1021/acssensors.8b00269
ACS Sens. 2018, 3, 1264−1270

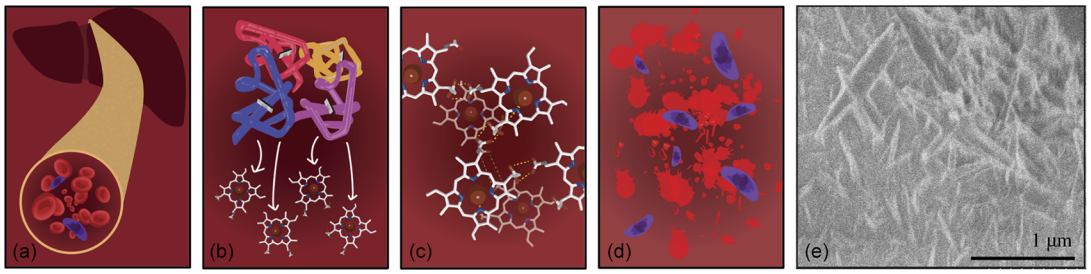

Figure 1. Hemozoin production. (a–d) Formation of hemozoin and subsequent release into the bloodstream. (a) Parasite (shown in purple) remains in the liver, reproducing until it is released into the bloodstream. (b) Free heme is generated, as a byproduct of hemoglobin consumption by the parasite. (c) Heme is aggregated into an insoluble crystal known as hemozoin. (d) Hemozoin is released into circulation during erythrocyte lysis. (e) Scanning electron microscopy image of β-hematin, a hemozoin mimic.

all other naturally occurring materials in the blood, hemozoin exhibits strong paramagnetic behavior, responding to low magnetic field strengths. Therefore, if found in a patient's blood, hemozoin is indicative of malarial infection.[31−33]

As shown in Figure 1, the malaria parasite uses hemoglobin as its primary nutrient source, leading to parasite growth and asexual replication while also generating monomeric heme, which is highly toxic to the parasite. As the parasite is unable to excrete the free heme and does not possess a heme oxygenase to recover the iron and detoxify the heme, heme is converted by the parasite in a crystallization process to form the insoluble hemozoin.[34,35] The morphology of hemozoin varies depending on the parasite species,[36,37] though the nanocrystals typically have an elongated rod-like shape with a length ranging from 300 nm to 1 μm.

Given hemozoin's specificity as an indicator for malaria, a wide range of methods have been developed for its detection. Two of the more popular methods with abilities to consistently detect clinically relevant concentrations of hemozoin are laser desorption mass spectrometry and Raman spectroscopy.[1,38−40] Other methods include flow cytometry and polarization microscopy.[41−44] However, similar to conventional smear optical imaging, these methods are time- and equipment-intensive and require extensive training on the part of the user to yield accurate results. In parallel with the development of these detection systems, a hemozoin mimic has been created, known as β-hematin, allowing for the study of hemozoin without the need to handle malaria-infected samples.[45] β-Hematin and hemozoin from *P. falciparum* share the same unit crystal structure and the same magnetic and optical properties, making β-hematin the standard hemozoin mimic used in the field.[36,46] In addition, the hemozoin crystals from other *Plasmodium* species that infect humans, specifically *P. vivax*, *P. ovale*, *P. malariae*, and *P. knowlesi*, are very similar to those from *P. falciparum*, making β-hematin a sufficient mimic for all forms of human malaria.[36,47]

Leveraging these unique properties of hemozoin, we have designed, constructed, and validated a portable optical diagnostic system (PODS) for malaria detection (Figure 2). The PODS is based on differential optical spectroscopy. Specifically, by monitoring the change in optical power before and after a magnet is applied, we are able to determine the concentration of β-hematin present in whole blood.

In the design of this system, we placed a strong emphasis on engineering for operation in low-resource environments with a goal of detecting clinically relevant concentrations in whole blood. Several considerations are taken into account when designing a diagnostic platform for operation in low-resource settings, including cost, weight, energy, reagents and disposable materials, system lifetime and part replacement, and user interface. Notably, our design and optimization process was focused on the end application and the target audience rather than achieving the ultimate sensitivity or performance possible.

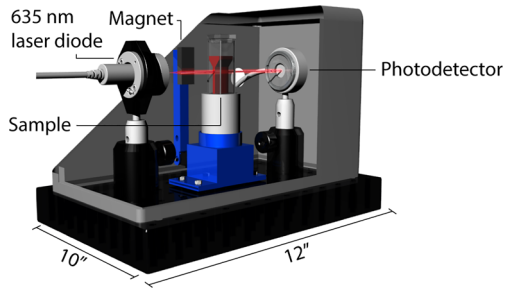

Figure 2. Schematic of the PODS. The entire PODS weighs 10 pounds and is enclosed in a dark plastic box to minimize noise from ambient light and increase portability. The PODS consists of off-the-shelf components that can be readily replaced, and it can operate strictly off of battery power for approximately 8 h of continuous use.

Light from a 635 nm laser diode (ThorLabs, CPS635) passes through a poly(methyl methacrylate) microcuvette containing 500 μL of sample to a photodetector (ThorLabs, S120C). To perform detection, a pair of measurements is taken with and without a magnet in close proximity to the sample. Because the magnet pulls all of the magnetic nanoparticles out of the beam path, the difference between the two signals is directly related to the nanoparticle concentration. This strategy is elegant in its simplicity as it reduces the effect of sample-to-sample variation, which is inherent in human specimens. The detection of clinically relevant concentration ranges (<1 to 5 μg/mL[15,48,49]) in whole blood with no additional reagents is demonstrated. Given this system design, all previous system design constraints are met, and the diagnostic platform is ideally suited for low-resource environments.

RESULTS AND DISCUSSION

System Optimization Experiments. Before performing measurements with whole blood, a series of measurements were performed to optimize several system design parameters including the magnetic field strength, sample size, and data acquisition time. A subset of these results is shown in Figure 3. Additional results, including system optimization experiments with nanoparticles and control experiments, are contained in the Supporting Information.

As expected, the signal is dependent on the concentration of β-hematin present in the solution. As shown in Figure 3a, at β-

DOI: 10.1021/acssensors.8b00269
ACS Sens. 2018, 3, 1264−1270

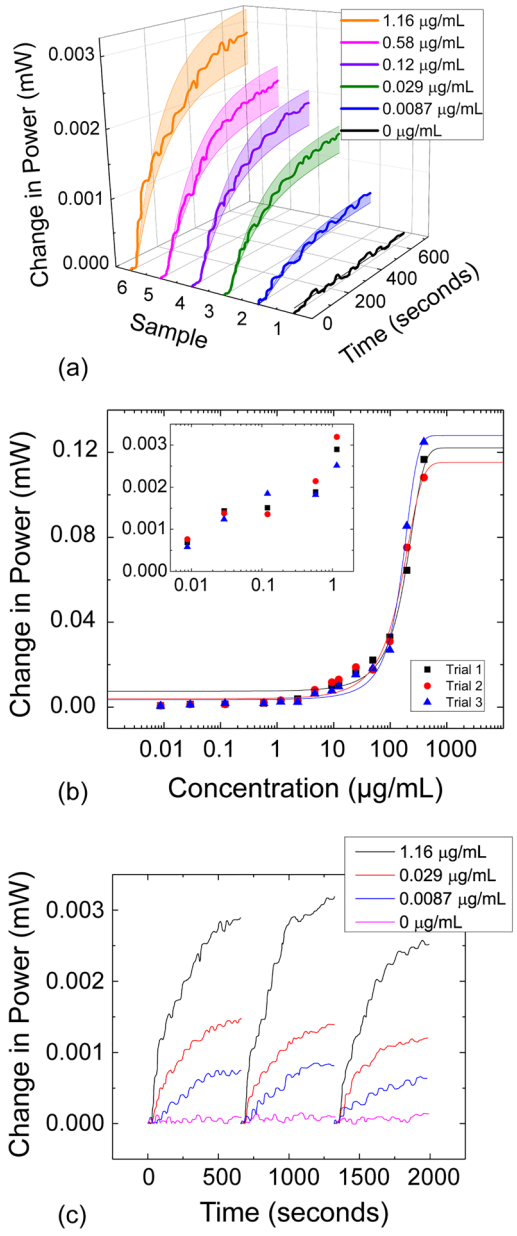

Figure 3. Results for preliminary tests with β-hematin in 10% PEG. (a) Experimental and mathematical results. Solid lines show experimental data; shaded regions show ranges provided by mathematical modeling. Time on the x-axis refers to the total testing time. The magnetic field is applied at t = 30 s. (b) Working range of the PODS for β-hematin concentrations in 10% PEG. (c) Reproducibility of results. The measurement was performed iteratively using the same setup.

hematin concentrations as low as 0.0087 μg/mL, we still see a sizable increase in transmission upon application of the magnetic field as compared to the base noise level (signal-to-noise ratio equals 5.03). There is also excellent agreement between the experimental data and the ranges provided by the simulations. The slight fluctuation in the transmission can be attributed to random particle−particle interactions. Because of the stochastic nature of these interactions, it was not possible to predict absolute values at any point in time. As such, to capture the overall transmission change due to the particle motion, lower and upper bounds on the signal were calculated, giving a ±15% bound around the model fitting results. By fitting the experimental data, the coefficients $f(\rho)$ and δ_1 are determined, and $f(\rho)$ fits a sigmoidal curve, as expected. Here, $f(\rho)$ is a function of the concentration of the particles, and δ_1 is related to the properties of the particles and the magnetic field. These two parameters are discussed in more detail in the methods and in the Supporting Information. Also, for the same type of particle, δ_1 is larger for solutions with lower viscosity, which agrees with its definition. The details of the model, including all constants used as well as derivations, are in the Supporting Information.

Figure 3b shows the characterization of the working range of the PODS, and Figure 3c investigates the reproducibility of the instrument. Each sample was analyzed three times to determine the reproducibility of the sensing signal generated. As can be seen in Figure 3c, the signal produced by the device is fairly consistent for each concentration tested. All of these results, along with additional preliminary experiments with iron oxide nanoparticles (included in the Supporting Information), confirmed that the PODS was capable of reproducibly detecting clinically relevant concentrations of β-hematin in PEG solutions with minimal user input.

β-Hematin in Blood Experiments. To verify the diagnostic abilities of the PODS system, a series of whole blood samples were doped with known concentrations of β-hematin and analyzed. Notably, only 500 μL of the sample is used in the analysis, and the only processing conducted on the sample is an ultrasound treatment. No additional reagents are needed. A subset of the results from the β-hematin measurements in whole blood is shown in Figure 4.

As shown in Figure 4a, the signal is dependent on the concentration of β-hematin present in the solution. At concentrations as low as 0.0081 μg/mL of β-hematin, we are still seeing a sizable increase in transmission upon application of the magnetic field as compared to the base noise level (signal-to-noise ratio equals 4.03). Additionally, the noise does not appreciably increase as the concentration increases. There is also excellent agreement between the experimental data and the ranges provided by the simulations. As with the previous results, lower and upper bounds give a ±15% range above and below the fitting results.

Figure 4b shows the characterization of the working range of the PODS. As expected, it has a sigmoidal response, though the entire sigmoid to the saturation point was unable to be captured. Although a sensitivity level of <1 μg/mL may seem unremarkable when taken in the broader context of ultrahigh sensitivity diagnostics, it is important to remember that the relevant detection concentrations for malaria are <1−5 μg/mL of hemozoin, which corresponds to <26 parasites/μL. Additionally, this device has shown the ability to detect concentrations a full order of magnitude below clinical relevance and still differentiate the signal from the noise.

Figure 4c investigates the reproducibility of the instrument's signal. Each sample was tested three times to monitor the behavior of the system over three separate cycles. As can be seen in Figure 4c, the signal produced by the PODS is fairly consistent over each cycle for the low and medium concentrations tested. However, at the very high concentration levels and after multiple measurements on the same sample, the change in signal begins to decrease, and the noise level increases. This behavior is attributed to the nanoparticles forming aggregates. This result verifies that the signal produced by the PODS is reproducible at clinically relevant concentrations, which is a key feature of a diagnostic tool.

DOI: 10.1021/acssensors.8b00269
ACS Sens. 2018, 3, 1264−1270

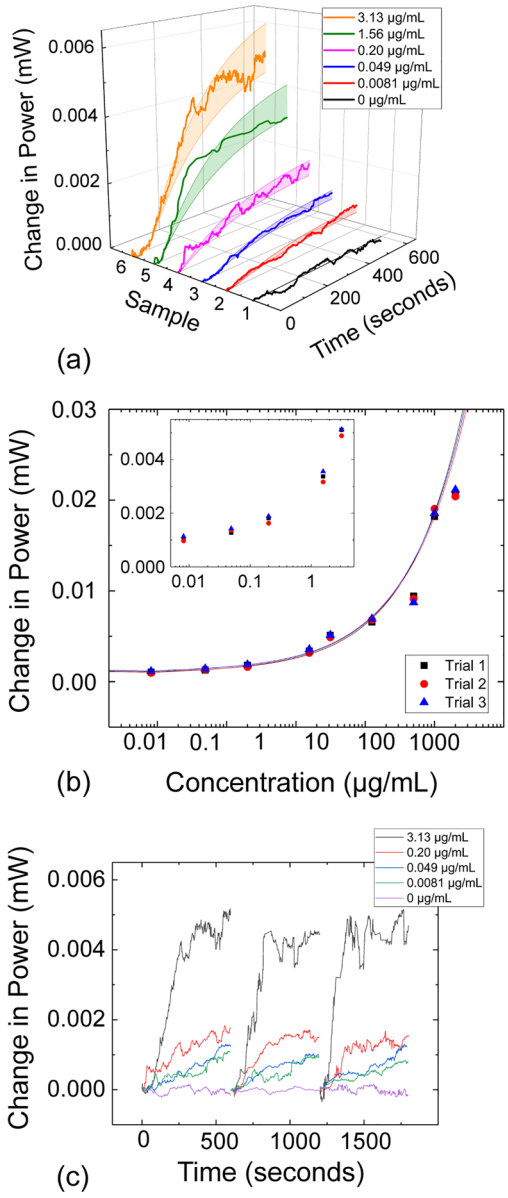

Figure 4. Results for tests with β-hematin in whole rabbit blood. (a) Experimental and mathematical results. Solid lines show experimental data; shaded regions show ranges provided by mathematical modeling. (b) Working range of the PODS for β-hematin concentrations in rabbit blood. (c) Reproducibility of results. The measurement was performed iteratively using the same setup.

In this work, we demonstrate an innovative and practical tool for malaria screening. We validated that, through the use of magneto-optic technology, we can detect clinically relevant concentrations of a hemozoin mimic in whole rabbit blood. Additionally, the size, weight, and power requirements of the PODS make it ideal for use in low-resource environments as a screening diagnostic.

Although this work confirmed the diagnostic mechanism and the sample compatibility, there are some experiments that must be performed before this device may be implemented in malaria-endemic regions. We must further validate the diagnostic ability using samples infected with malaria and conduct a longitudinal study to see how the specificity and sensitivity of the PODS changes through the course of the natural disease progression (and through the course of subsequent treatment).

In conclusion, we have developed a portable, self-contained malaria diagnostic capable of detecting clinically relevant concentrations of synthetic hemozoin in 500 μL of whole rabbit blood, and we have verified the device's functionality with both mathematical modeling and experiments. The PODS has shown the ability to detect concentrations of a synthetic hemozoin mimic a full order of magnitude below clinical relevance, while still differentiating the signal from the noise. Although 500 μL is not likely to be achievable with a finger prick, presently, further work is being conducted to decrease the sample volume required by reconfiguring the sample cuvette and exploring alternative photodetectors. In addition, whereas this system utilizes ultrasound to lyse the blood samples, there are many other methods known to lyse cells that could be more readily incorporated into the system, all of which are being tested and considered for future versions of the PODS. By identifying both asymptomatic and symptomatic populations in malaria-endemic regions, early stage diagnosis and therapeutic intervention can occur, both of which are crucial to successfully eliminate this disease.

METHODS

Experimental Strategy. The goal of this study was to validate the PODS using whole blood samples, confirming both the magneto-optic detection mechanism and its compatibility with untreated whole blood samples. The ability to detect malaria without costly and delicate reagents could be transformative in combatting the disease in low-resource regions.

To reduce potential confounds and enable precise control over the concentration of nanoparticle in the blood, we opted to work with β-hematin, an exact mimic of hemozoin, the byproduct created by the parasite that the PODS is designed to detect. We first conducted experiments to optimize the system, testing a wide range of concentrations of β-hematin in solvents with viscosities similar to blood. Once the PODS was optimized, we tested β-hematin in whole rabbit blood samples. No additional reagents were required, and the only processing step was ultrasound treatment of the samples to lyse the cells. Each sample was tested at least three times to ensure reproducibility.

Synthesis of β-Hematin by Acetate-Mediated Production. To synthesize β-hematin, we followed the standard acetate-mediated production route.[30,50] Hemin (90 mg, Fluka) was dissolved in 10 mL of NaOH (0.1 M) and neutralized with 1 mL of HCl (1 M). To this was added 9.25 mL of acetate buffer (9.7 M, pH 4.8), and the mixture was incubated for 1 h at 60 °C. After incubation, the reaction was quenched with water, and the mixture was cooled over ice. The resulting precipitate was collected via filtration and extensively washed with water. To remove any unreacted hemin, the air-dried precipitate was placed in a 15 mL Falcon tube with 1 mL of an aqueous pyridine solution consisting of 5% (v/v) pyridine, 40% (v/v) acetone, and 0.02 M HEPES (pH 7.4). This well-shaken mixture was diluted to 10 mL with water, centrifuged for 10 min, and the supernatant discarded. The resulting precipitate was washed with water until the supernatant was clear. Finally, the precipitate was collected via filtration and left to dry over P_2O_5.

Device Design. As shown in Figure 2, light from a 635 nm laser diode (ThorLabs, CPS635) passes through a 3 mL poly(methyl methacrylate) microcuvette to a photodetector (ThorLabs, S120C). To perform detection, a magnet is brought in close proximity to the sample using a motorized linear actuator. The magnet pulls all of the magnetic nanoparticles out of the beam path, thereby increasing the optical transparency of the solution. The change in optical power is recorded and plotted in real-time on a laptop. The PODS weighs 10 pounds and is entirely self-contained within a dark plastic box, which not only increases portability but also decreases the effects of ambient

DOI: 10.1021/acssensors.8b00269
ACS Sens. 2018, 3, 1264−1270

light on the system. The PODS can operate strictly off of battery power for approximately 8 h of continuous use. The limiting factor is the laptop to which the data are output. Otherwise, the only component that requires charging is the laser diode, which can be powered by an external USB battery pack for up to 36 h.

It is important to note that the magnet is initially located sufficiently far from the sample, such that the magnetic field (B) is negligible inside the cuvette. By decreasing the gap distance between the magnet and the sample, the magnetic field strength increases. In the present work, this gap was decreased quickly enough that the magnetic field strength had two states: on and off. This approach allows label-free detection of the nanoparticles to be performed in real-time as well as self-normalization. Initial experiments contained in the supplement optimized the magnet strength, which, in turn, determined the PODS footprint and the detection time. Specifically, a stronger magnet decreases the time-to-signal, enabling higher sample throughput. However, a stronger magnet also increases the requisite initial gap distance between the sample and the magnet, increasing the system footprint. For the present work, the magnet strength was chosen such that sample throughput was one sample every 8−10 min with an overall footprint under 10 in. × 12 in.

Mathematical Modeling. To understand the sensing signal, a mathematical model was created. Although the model is based on optical spectroscopy, it also incorporates the time-dependent nature of the signal that arises from the interaction of the magnetic field with the magnetic nanoparticles. As has been well established, the optical signal in optical transmission spectroscopy is primarily due to scattering and absorption.[51,52] In the present work, the signal is dominated by the scattering component. As such, the power of the transmitted light is inversely related to the number of particles in the path of the laser beam.

To model the signal generated, first, the trajectories of the nanoparticles are calculated. Once these values are known, the number of nanoparticles in the path of the laser beam and the induced optical transmission decrease at any point in time can be determined. The particle motion can be described by 2D equations of motion that describe the horizontal (x) and vertical (y) directions. By solving the equations of motion, the expression for the change in transmitted power (ΔP) versus time can be derived as

$$\Delta P = f(\rho)(1 - e^{-\delta_1 t})$$

where $f(\rho)$ is a function of the density of the magnetic nanoparticle, which reveals the maximum power in transmission that can be detected for different concentrations of nanoparticles. The effects of magnetic force and viscosity are captured in δ_1, which is defined in Supporting Information, and t is time.

β-Hematin in PEG Measurements. To optimize parameters and validate the diagnostic capability of the PODS, we first performed a series of measurements with rod-shaped β-hematin (75 nm × 75 nm × 300−400 nm,[36] as shown in Figure 1e). Particles were suspended in 10% polyethylene glycol (PEG) and 15% PEG. The addition of PEG increased the viscosity of the solution in a predictable manner, allowing validation of a mathematical model. Using serial dilution, a range of concentrations of each solution was made from 393.3 to 0.0087 μg/mL. Each sample was then analyzed using the PODS in the same manner. First, a background was taken using a null or blank solution (10 or 15% PEG, dependent upon the sample). Then, 3 mL of the sample was pipetted into an empty cuvette, and with the magnet located away from the sample, the box was closed. A second background was taken for 30 s to compare with the initial background to ensure that changing the samples had not disrupted the system, and then the magnet was moved into place using the motorized stage. Notably, the box was not moved during either of these measurements, enabling the continuous acquisition of data and observation of the onset of magnetic field-induced nanoparticle motion. The total measurement duration was 10 min with an acquisition rate of 60 points/min, for a total of 600 points/measurement. All measurements were performed multiple times (N = 3) on the same solution to verify reproducibility of the measurement.

β-Hematin in Whole Rabbit Blood Measurements. To validate the diagnostic capability of the PODS and verify the model in blood samples, we performed a series of measurements with β-hematin suspended in whole blood, collected from live Dutch Belted rabbits and mixed with anticoagulant (Camco Sequester-Sol Liquid Anticoagulant) to prevent clotting during transportation to the lab. A series of solutions was then made, resuspending the β-hematin particles in whole blood at 4.0 mg/mL concentration. Using serial dilution, a range of concentrations was made from 400 to 0.0081 μg/mL. Each sample was then lysed by sonication for 60 s[53] and analyzed using the PODS in the same manner. First, a background was taken using a null, or blank, solution (uninfected rabbit blood). Then, 500 μL of the sample was pipetted into an empty microcuvette, and with the magnet located away from the sample, the box was closed. A second background was taken for 30 s to compare with the initial background to ensure that changing the samples had not disrupted the system, and then the magnet was moved into place using the motorized stage. Notably, the box was not moved during either of these measurements, enabling the continuous acquisition of data and observation of the onset of magnetic field-induced nanoparticle motion. The total measurement duration was 10 min with an acquisition rate of 60 points/min, for a total of 600 points/measurement. All measurements are performed multiple times (N = 3) on the same solution to verify reproducibility of the measurement.

■ ASSOCIATED CONTENT

Supporting Information

The Supporting Information is available free of charge on the ACS Publications website at DOI: 10.1021/acssensors.8b00269.

Mathematical modeling, synthesis of Fe_3O_4 nanoparticles by chemical coprecipitation, optimization of magnetic strength and detection time, Fe_3O_4 nanoparticle testing results, β-hematin testing results in polyethylene glycol, β-hematin testing results in rabbit blood (PDF)

■ AUTHOR INFORMATION

Corresponding Author

*E-mail: armani@usc.edu.

ORCID

Dongyu Chen: 0000-0001-8473-2804

Andrea M. Armani: 0000-0001-9890-5104

Author Contributions

S.E.M. designed and patented the device, synthesized nanoparticles, performed experiments, and analyzed data. D.C. developed the mathematical models. A.S. wrote and maintained all of the codes for the device to function as intended. H.A. was responsible for maintaining the animal facility and providing SEM with rabbit blood. A.M.A. aided in experimental and instrument design and data analysis. The manuscript was written through contributions of all authors. All authors have given approval to the final version of the manuscript.

Notes

The authors declare no competing financial interest.

■ ACKNOWLEDGMENTS

The authors would like to thank Andre Kovach, Martin Siron, and Josh Neutel for helping with iron oxide nanoparticle synthesis and β-hematin synthesis; Dr. Timothy Egan for troubleshooting issues encountered with β-hematin synthesis; Vinh Diep for helping obtain SEM images of the β-hematin; Amirmohsen Arbabi for working with Samantha to obtain rabbit blood; IDEO Design Innovation Workshop and the IEEE Healthcare Innovation and Point-of-Care Technologies

DOI: 10.1021/acssensors.8b00269
ACS Sens. 2018, 3, 1264−1270

Conference for planting the seed for this project. This project was funded by the Alfred E. Mann Innovation in Engineering Doctoral Fellowship, Office of Naval Research (N00014-17-2270, N00014-15-1-2703), and Health, Technology, and Engineering (HTE) program.

REFERENCES

(1) Demirev, P. A. Mass spectrometry for malaria diagnosis. *Expert Rev. Mol. Diagn.* **2004**, *4* (6), 821−829.
(2) Breman, J. G.; Alilio, M. S.; Mills, A. Conquering the intolerable burden of malaria: what's new, what's needed: a summary. *Am. J. Trop. Med. Hyg* **2004**, *71* (2 Suppl), 1−15.
(3) Guerin, P. J.; Olliaro, P.; Nosten, F.; Druilhe, P.; Laxminarayan, R.; Binka, F.; Kilama, W. L.; Ford, N.; White, N. J. Malaria: current status of control, diagnosis, treatment, and a proposed agenda for research and development. *Lancet Infect. Dis.* **2002**, *2* (9), 564−73.
(4) Kager, P. A. Malaria control: constraints and opportunities. *Trop. Med. Int. Health* **2002**, *7* (12), 1042−6.
(5) Morens, D. M.; Folkers, G. K.; Fauci, A. S. The challenge of emerging and re-emerging infectious diseases. *Nature* **2004**, *430* (6996), 242−9.
(6) Phillips, R. S. Current status of malaria and potential for control. *Clin Microbiol Rev.* **2001**, *14* (1), 208−26.
(7) World Health Organization. *World malaria report 2016*; World Health Organization: Geneva, 2016.
(8) Nabarro, D.; Mendis, K. *Roll Back Malaria is unarguably both necessary and possible [round table discussion]*, 2000.
(9) World Health Organization. *Roll Back Malaria highlights 2000−2001*; WHO Regional Office for Europe: Copenhagen, 2002.
(10) Mayor, A.; Bardají, A.; Macete, E.; Nhampossa, T.; Fonseca, A. M.; González, R.; Maculuve, S.; Cisteró, P.; Rupérez, M.; Campo, J.; et al. Changing trends in P. falciparum burden, immunity, and disease in pregnancy. *N. Engl. J. Med.* **2015**, *373* (17), 1607−1617.
(11) Ciminera, P.; Brundage, J. Malaria in U.S. military forces: a description of deployment exposures from 2003 through 2005. *Am. J. Trop. Med. Hyg* **2007**, *76* (2), 275−9.
(12) Greenwood, B. The molecular epidemiology of malaria. *Trop. Med. Int. Health* **2002**, *7* (12), 1012−21.
(13) Makler, M. T.; Palmer, C. J.; Ager, A. L. A review of practical techniques for the diagnosis of malaria. *Ann. Trop. Med. Parasitol.* **1998**, *92* (4), 419−33.
(14) Reyburn, H.; Mbatia, R.; Drakeley, C.; Carneiro, I.; Mwakasungula, E.; Mwerinde, O.; Saganda, K.; Shao, J.; Kitua, A.; Olomi, R.; Greenwood, B. M.; Whitty, C. J. Overdiagnosis of malaria in patients with severe febrile illness in Tanzania: a prospective study. *BMJ.* **2004**, *329* (7476), 1212.
(15) Butykai, A.; Orban, A.; Kocsis, V.; Szaller, D.; Bordacs, S.; Tatrai-Szekeres, E.; Kiss, L. F.; Bota, A.; Vertessy, B. G.; Zelles, T.; Kezsmarki, I. Malaria pigment crystals as magnetic micro-rotors: key for high-sensitivity diagnosis. *Sci. Rep.* **2013**, *3*, 1431.
(16) Bigaillon, C.; Fontan, E.; Cavallo, J. D.; Hernandez, E.; Spiegel, A. Ineffectiveness of the Binax NOW malaria test for diagnosis of Plasmodium ovale malaria. *J. Clin Microbiol* **2005**, *43* (2), 1011.
(17) Dimaio, M. A.; Pereira, I. T.; George, T. I.; Banaei, N. Performance of BinaxNOW for diagnosis of malaria in a U.S. hospital. *J. Clin Microbiol* **2012**, *50* (9), 2877−80.
(18) Mboera, L. E.; Fanello, C. I.; Malima, R. C.; Talbert, A.; Fogliati, P.; Bobbio, F.; Molteni, F. Comparison of the Paracheck-Pf test with microscopy, for the confirmation of Plasmodium falciparum malaria in Tanzania. *Ann. Trop. Med. Parasitol.* **2006**, *100* (2), 115−22.
(19) Moody, A. Rapid diagnostic tests for malaria parasites. *Clin Microbiol Rev.* **2002**, *15* (1), 66−78.
(20) Murray, C. K.; Bell, D.; Gasser, R. A.; Wongsrichanalai, C. Rapid diagnostic testing for malaria. *Trop. Med. Int. Health* **2003**, *8* (10), 876−83.
(21) Gamboa, D.; Ho, M. F.; Bendezu, J.; Torres, K.; Chiodini, P. L.; Barnwell, J. W.; Incardona, S.; Perkins, M.; Bell, D.; McCarthy, J.; Cheng, Q. A large proportion of P. falciparum isolates in the Amazon region of Peru lack pfhrp2 and pfhrp3: implications for malaria rapid diagnostic tests. *PLoS One* **2010**, *5* (1), e8091.
(22) Ashley, E. A.; Touabi, M.; Ahrer, M.; Hutagalung, R.; Htun, K.; Luchavez, J.; Dureza, C.; Proux, S.; Leimanis, M.; Lwin, M. M.; Koscalova, A.; Comte, E.; Hamade, P.; Page, A. L.; Nosten, F.; Guerin, P. J. Evaluation of three parasite lactate dehydrogenase-based rapid diagnostic tests for the diagnosis of falciparum and vivax malaria. *Malar. J.* **2009**, *8*, 241.
(23) World Health Organization. *False-negative RDT results and implications of new reports of P. falciparum histidine-rich protein 2/3 gene deletions*; World Health Organization: Geneva, 2017.
(24) Egan, T. J.; Chen, J. Y. J.; de Villiers, K. A.; Mabotha, T. E.; Naidoo, K. J.; Ncokazi, K. K.; Langford, S. J.; McNaughton, D.; Pandiancherri, S.; Wood, B. R. Haemozoin (beta-haematin) biomineralization occurs by self-assembly near the lipid/water interface. *FEBS Lett.* **2006**, *580* (21), 5105−5110.
(25) Egan, T. J. Haemozoin formation. *Mol. Biochem. Parasitol.* **2008**, *157* (2), 127−136.
(26) Newman, D. M.; Heptinstall, J.; Matelon, R. J.; Savage, L.; Wears, M. L.; Beddow, J.; Cox, M.; Schallig, H.; Mens, P. F. A magneto-optic route toward the in vivo diagnosis of malaria: Preliminary results and preclinical trial data. *Biophys. J.* **2008**, *95* (2), 994−1000.
(27) Weissbuch, I.; Leiserowitz, L. Interplay Between Malaria, Crystalline Hemozoin Formation, and Antimalarial Drug Action and Design. *Chem. Rev.* **2008**, *108* (11), 4899−4914.
(28) Parroche, P.; Lauw, F. N.; Goutagny, N.; Latz, E.; Monks, B. G.; Visintin, A.; Halmen, K. A.; Lamphier, M.; Olivier, M.; Bartholomeu, D. C.; Gazzinelli, R. T.; Golenbock, D. T. Malaria hemozoin is immunologically inert but radically enhances innate responses by presenting malaria DNA to Toll-like receptor 9. *Proc. Natl. Acad. Sci. U. S. A.* **2007**, *104* (6), 1919−1924.
(29) Bernabeu, M.; Danziger, S. A.; Avril, M.; Vaz, M.; Babar, P. H.; Brazier, A. J.; Herricks, T.; Maki, J. N.; Pereira, L.; Mascarenhas, A.; et al. Severe adult malaria is associated with specific PfEMP1 adhesion types and high parasite biomass. *Proc. Natl. Acad. Sci. U. S. A.* **2016**, *113* (23), E3270−E3279.
(30) Ambele, M. A.; Sewell, B. T.; Cummings, F. R.; Smith, P. J.; Egan, T. J. Synthetic Hemozoin (beta-Hematin) Crystals Nucleate at the Surface of Neutral Lipid Droplets that Control Their Sizes. *Cryst. Growth Des.* **2013**, *13* (10), 4442−52.
(31) Gluzman, I. Y.; Francis, S. E.; Oksman, A.; Smith, C. E.; Duffin, K. L.; Goldberg, D. E. Order and specificity of the Plasmodium falciparum hemoglobin degradation pathway. *J. Clin. Invest.* **1994**, *93* (4), 1602−8.
(32) Goldberg, D. E.; Slater, A. F.; Cerami, A.; Henderson, G. B. Hemoglobin degradation in the malaria parasite Plasmodium falciparum: an ordered process in a unique organelle. *Proc. Natl. Acad. Sci. U. S. A.* **1990**, *87* (8), 2931−5.
(33) Inyushin, M.; Kucheryavih, Y.; Kucheryavih, L.; Rojas, L.; Khmelinskii, I.; Makarov, V. Superparamagnetic Properties of Hemozoin. *Sci. Rep.* **2016**, *6*, 26212.
(34) Egan, T. J. Recent advances in understanding the mechanism of hemozoin (malaria pigment) formation. *J. Inorg. Biochem.* **2008**, *102* (5−6), 1288−99.
(35) Slater, A. F.; Swiggard, W. J.; Orton, B. R.; Flitter, W. D.; Goldberg, D. E.; Cerami, A.; Henderson, G. B. An iron-carboxylate bond links the heme units of malaria pigment. *Proc. Natl. Acad. Sci. U. S. A.* **1991**, *88* (2), 325−9.
(36) Noland, G. S.; Briones, N.; Sullivan, D. J., Jr. The shape and size of hemozoin crystals distinguishes diverse Plasmodium species. *Mol. Biochem. Parasitol.* **2003**, *130* (2), 91−9.
(37) Oliveira, M. F.; Kycia, S. W.; Gomez, A.; Kosar, A. J.; Bohle, D. S.; Hempelmann, E.; Menezes, D.; Vannier-Santos, M. A.; Oliveira, P. L.; Ferreira, S. T. Structural and morphological characterization of hemozoin produced by Schistosoma mansoni and Rhodnius prolixus. *FEBS Lett.* **2005**, *579* (27), 6010−6.
(38) Demirev, P. A.; Feldman, A. B.; Kongkasuriyachai, D.; Scholl, P.; Sullivan, D., Jr.; Kumar, N. Detection of malaria parasites in blood by

DOI: 10.1021/acssensors.8b00269
ACS Sens. 2018, 3, 1264−1270

laser desorption mass spectrometry. *Anal. Chem.* **2002**, *74* (14), 3262−6.
(39) Hobro, A. J.; Konishi, A.; Coban, C.; Smith, N. I. Raman spectroscopic analysis of malaria disease progression via blood and plasma samples. *Analyst* **2013**, *138* (14), 3927−33.
(40) Scholl, P. F.; Kongkasuriyachai, D.; Demirev, P. A.; Feldman, A. B.; Lin, J. S.; Sullivan, D. J., Jr.; Kumar, N. Rapid detection of malaria infection in vivo by laser desorption mass spectrometry. *Am. J. Trop. Med. Hyg* **2004**, *71* (5), 546−51.
(41) Burnett, J. L.; Carns, J. L.; Richards-Kortum, R. In vivo microscopy of hemozoin: towards a needle free diagnostic for malaria. *Biomed. Opt. Express* **2015**, *6* (9), 3462−74.
(42) Delahunt, C.; Horning, M. P.; Wilson, B. K.; Proctor, J. L.; Hegg, M. C. Limitations of haemozoin-based diagnosis of Plasmodium falciparum using dark-field microscopy. *Malar. J.* **2014**, *13*, 147.
(43) Jun, G.; Lee, J. S.; Jung, Y. J.; Park, J. W. Quantitative determination of Plasmodium parasitemia by flow cytometry and microscopy. *J. Korean Med. Sci.* **2012**, *27* (10), 1137−42.
(44) Rebelo, M.; Sousa, C.; Shapiro, H. M.; Mota, M. M.; Grobusch, M. P.; Hanscheid, T. A novel flow cytometric hemozoin detection assay for real-time sensitivity testing of Plasmodium falciparum. *PLoS One* **2013**, *8* (4), e61606.
(45) Sandlin, R. D.; Fong, K. Y.; Stiebler, R.; Gulka, C. P.; Nesbitt, J. E.; Oliveira, M. P.; Oliveira, M. F.; Wright, D. W. Detergent-Mediated Formation of beta-Hematin: Heme Crystallization Promoted by Detergents Implicates Nanostructure Formation for Use as a Biological Mimic. *Cryst. Growth Des.* **2016**, *16* (5), 2542−2551.
(46) Jaramillo, M.; Bellemare, M. J.; Martel, C.; Shio, M. T.; Contreras, A. P.; Godbout, M.; Roger, M.; Gaudreault, E.; Gosselin, J.; Bohle, D. S.; Olivier, M. Synthetic Plasmodium-like hemozoin activates the immune response: a morphology - function study. *PLoS One* **2009**, *4* (9), e6957.
(47) Joyner, C.; Moreno, A.; Meyer, E. V.; Cabrera-Mora, M.; Kissinger, J. C.; Barnwell, J. W.; Galinski, M. R. Plasmodium cynomolgi infections in rhesus macaques display clinical and parasitological features pertinent to modelling vivax malaria pathology and relapse infections. *Malar. J.* **2016**, *15* (1), 451.
(48) Chen, K.; Yuen, C.; Aniweh, Y.; Preiser, P.; Liu, Q. Towards ultrasensitive malaria diagnosis using surface enhanced Raman spectroscopy. *Sci. Rep.* **2016**, *6*, 20177.
(49) Newman, D. M.; Heptinstall, J.; Matelon, R. J.; Savage, L.; Wears, M. L.; Beddow, J.; Cox, M.; Schallig, H. D.; Mens, P. F. A magneto-optic route toward the in vivo diagnosis of malaria: preliminary results and preclinical trial data. *Biophys. J.* **2008**, *95* (2), 994−1000.
(50) Kuter, D.; Mohunlal, R.; Fitzroy, S.-M.; Asher, C.; Smith, P. J.; Egan, T. J.; de Villiers, K. A. Insights into the initial stages of lipid-mediated haemozoin nucleation. *CrystEngComm* **2016**, *18* (27), 5177−5187.
(51) Peticolas, W. L.; Fanconi, B.; Tomlinson, B.; Nafie, L. A.; Small, W. Inelastic light scattering from biological and synthetic polymers. *Ann. N. Y. Acad. Sci.* **1969**, *168* (3), 564−88.
(52) Smith, R. G. Optical power handling capacity of low loss optical fibers as determined by stimulated Raman and brillouin scattering. *Appl. Opt.* **1972**, *11* (11), 2489−94.
(53) Brown, R. B.; Audet, J. Current techniques for single-cell lysis. *J. R. Soc., Interface* **2008**, *5* (Suppl 2), S131−8.

DOI: 10.1021/acssensors.8b00269
ACS Sens. 2018, 3, 1264−1270